Redox active Ni-Pd carbonyl alloy nanoclusters: syntheses, molecular structures and electrochemistry of [Ni22-xPd20+x(CO)48]6-(x= 0.62), [Ni29-xPd6+x(CO)42]6-(x= 0.09) and [Ni29+xPd6-x(CO)42]6-(x= 0.27)

Redox Active Ni-Pd Carbonyl Alloy Nanoclusters: Syntheses, Molecular Structures and Electrochemistry of $[Ni_{22-x}Pd_{20+x}(CO)_{48}]^{6-}$ (x = 0.62), $[Ni_{29-x}Pd_{6+x}(CO)_{42}]^{6-}$ (x = 0.09) and $[Ni_{29+x}Pd_{6-x}(CO)_{42}]^{6-}$ (x = 0.27)

Beatrice Berti,[a] Cristiana Cesari,[a] Cristina Femoni,[a] Tiziana Funaioli,[b] Maria Carmela Iapalucci[a] and Stefano Zacchini[a]*

[a] Dipartimento di Chimica Industriale "Toso Montanari", Università di Bologna, Viale Risorgimento 4, 40136 Bologna. Italy. E-mail: stefano.zacchini@unibo.it

[b] Dipartimento di Chimica e Chimica Industriale, Università di Pisa, Via G. Moruzzi 13, 56124, Pisa, Italy

ABSTRACT

The redox active Ni-Pd alloy nanocluster $[Ni_{22-x}Pd_{20+x}(CO)_{48}]^{6-}$ (x = 0.62) ($[\mathbf{1}]^{6-}$) was obtained from the redox condensation of $[NBu_4]_2[Ni_6(CO)_{12}]$ with 0.7-0.8 equivalents of $Pd(Et_2S)_2Cl_2$ in CH_2Cl_2. Conversely, $[Ni_{29-x}Pd_{6+x}(CO)_{42}]^{6-}$ (x = 0.09) ($[\mathbf{2}]^{6-}$) and $[Ni_{29+x}Pd_{6-x}(CO)_{42}]^{6-}$ (x = 0.27) ($[\mathbf{3}]^{6-}$) were obtained employing $[NEt_4]_2[Ni_6(CO)_{12}]$ and 0.6-0.7 equivalents of $Pd(Et_2S)_2Cl_2$ in CH_3CN. The molecular structures of these high nuclearity Ni-Pd carbonyl clusters were determined by single-crystal X-ray diffraction (SC-XRD). $[\mathbf{1}]^{6-}$ adopted a M_{40} *ccp* structure comprising five close-packed ABCAB layers capped by two further Ni atoms. Conversely, $[\mathbf{2}]^{6-}$ and $[\mathbf{3}]^{6-}$displayed a *hcp* M_{35} metal core composed of three compact ABA layers. $[\mathbf{1}]^{6-}$, $[\mathbf{2}]^{6-}$ and $[\mathbf{3}]^{6-}$ reached nanometric sizes, being the maximum lengths of their metal cores 1.3 nm ($[\mathbf{1}]^{6-}$) and 1.0 nm ($[\mathbf{2}]^{6-}$ and $[\mathbf{3}]^{6-}$), that increased up to 1.9 and 1.5 nm, after including also the CO ligands. The Ni-Pd distribution within their metal cores was dictated by avoiding terminal Pd-CO bonding and minimizing Pd-CO coordination. As a consequence, site preference and partial metal segregation was observed, as well as some substitutional and compositional disorder. Electrochemical and spectroelectrochemical studies revealed that $[\mathbf{1}]^{6-}$ and $[\mathbf{2}]^{6-}$ were redox active and displayed four and three, respectively, stable oxidations states. Even though several redox active high nuclearity metal carbonyl clusters were previously reported, the results herein described represented the first examples of redox active Ni-Pd carbonyl alloy nanoclusters.

Introduction

Palladium is the only late transition metal that does not form homoleptic homometallic carbonyl clusters of the general type $[Pd_x(CO)_y]^{n-}$ (x, y > 1; n> 0).[1,2] This is due to weak Pd-Pd and Pd-CO(terminal) bonding. Indeed, Pd-Pd bonds are the weakest metal-metal bonds in the iron, cobalt and nickel triads.[3] Moreover, the high $5s^04d^{10}$ to $5s^14d^9$ promotion energy of atomic palladium (0.95 eV) greatly reduces Pd(dπ)–CO(π*) back-bonding.[2] A few cationic Pd-carbonyl complexes have been obtained in super-acidic media, whose stability relies solely in the enhanced Pd-CO σ-bonding.[4] Alternatively, several neutral or anionic heteroleptic CO/PR_3 Pd clusters have been reported, which systematically contain only bridging CO ligands, whereas terminal positions are occupied by phosphines.[5,6] This is in keeping with the fact that Pd surfaces coordinate CO only as a bridged adsorbate.[7] Similarly, several homoleptic bimetallic carbonyl anionic clusters are known and, in none of them, CO is terminally bonded to Pd.[8,9] Among these, a few high nuclearity Ni-Pd carbonyl clusters have been fully characterized, that is $[Ni_{36}Pd_8(CO)_{48}]^{6-}$,[10] $[Ni_{13}Pd_{13}(CO)_{34}]^{4-}$,[11] $[Ni_{16}Pd_{16}(CO)_{40}]^{4-}$ and $[Ni_{26}Pd_{20}(CO)_{54}]^{6-}$.[12] It must be remarked that, even if, contrary to Pd, Ni forms neutral and anionic homoleptic carbonyls, such chemistry is limited to low nuclearity clusters, such as $[Ni_6(CO)_{12}]^{2-}$, $[Ni_9(CO)_{18}]^{2-}$ and $[H_{4-n}Ni_{12}(CO)_{21}]^{4-}$ (n = 2-4).[13] Thus, the formation of larger Ni-Pd clusters results from the synergy between a metal reluctant to form carbonyls (Pd) and another that by itself affords only lower nuclearity clusters. Related synergic effects are very important in Ni-Pd nanoparticles and nanoclusters that find several applications in catalysis.[14-16]

From a structural point of view, high nuclearity Ni-Pd carbonyl clusters display complete or partial segregation of the two metals.[10-12] Both phenomena arise from avoiding terminal Pd-CO bonding and minimizing Pd-CO coordination, in general. Partial segregation may result in substitutional and/or compositional disorder.[10-12,17] Substitutional disorder indicates a compound with a well-defined Ni-Pd composition, in which some metal sites can be occupied either by Ni or Pd. In most of the cases known, within the metal cage of the cluster, there are some positions which are fully occupied by Ni, some positions which are fully occupied by Pd and some positions which are disordered Ni-Pd. In the case of compositional disorder, in addition to substitutional disorder, the overall Ni-Pd composition of the cluster is the result of a mixture of a few isostructural species differing for a few Ni/Pd atoms. A random Ni/Pd occupation of all metal sites would result in a random alloy nanocluster.

Because of the molecular nature of such nanoclusters, these phenomena can be fully unraveled by means of single-crystal X-ray diffraction (SC-XRD).[8,18-25] Thus, molecular alloy nanoclusters may contribute to the understanding of mixing and synergetic effects induced by alloying with atomic precision.[26,27] This might be of some significance also in interpreting metal migration, chemiadsorption and catalytic behavior of Ni-Pd alloy particles.[10,28,29] However, a larger amount of molecular alloy nanoclusters must be produced for these purposes.

In addition, large molecular metal carbonyl clusters behave often as electron sponge and can be defined multivalent, when they have at least three electrochemically reversible or quasi-reversible redox state sufficiently long lived to enable spectroscopic characterization.[8] For instance, a rich electrochemistry was documented for bimetallic Ni-Pt clusters such as $[H_{6-n}Ni_{38}Pt_6(CO)_{48}]^{n-}$ (n = 4-6),[30] $[H_{6-n}Ni_{35}Pt_9(CO)_{48}]^{n-}$ (n = 5-6),[10] $[H_{6-n}Ni_{36}Pt_4(CO)_{45}]^{n-}$ (n = 5-6), $[H_{6-n}Ni_{37}Pt_4(CO)_{46}]^{n-}$ (n = 5-6),[31] and $[HNi_{24}Pt_{14}(CO)_{44}]^{5-}$,[8] and their electron-sink properties were ascertained. Conversely, the electrochemical behaviour of related Ni-Pd carbonyl clusters was not reported, or only preliminary data were described.[5,8,10] For instance, $[Ni_{13}Pd_{13}(CO)_{34}]^{4-}$ was found to undergo only irreversible redox processes.[10] Thus, it is also interesting to study in detail the electrochemical behaviour of large Ni-Pd molecular nanoclusters.

Herein we report the syntheses of the new molecular alloy nanoclusters $[Ni_{22-x}Pd_{20+x}(CO)_{48}]^{6-}$ (x = 0.62) ([**1**]$^{6-}$), $[Ni_{29-x}Pd_{6+x}(CO)_{42}]^{6-}$ (x = 0.09) ([**2**]$^{6-}$) and $[Ni_{29+x}Pd_{6-x}(CO)_{42}]^{6-}$ (x = 0.27) ([**3**]$^{6-}$). Their syntheses is based on the redox condensation of $[Ni_6(CO)_{12}]^{2-}$ with Pd(II) compounds, and strongly depends on the stoichiometry and the solvent employed. The total structures of these new clusters have been determined by SC-XRD and their redox behaviour investigated by means of electrochemical and spectroelectrochemical methods.

Results and Discussion

Synthesis and structure of $[Ni_{22-x}Pd_{20+x}(CO)_{48}]^{6-}$ (x = 0.62) ([1]$^{6-}$)

[**1**]$^{6-}$ was obtained from the reaction of $[NBu_4]_2[Ni_6(CO)_{12}]$ with 0.7-0.8 equivalents of $Pd(Et_2S)_2Cl_2$ in CH_2Cl_2 and extracted in acetone after work-up (see Experimental for details). Formation of [**1**]$^{6-}$ was accompanied by significant amounts of $Ni(CO)_4$ and Ni^{2+} salts as side products. The anion[**1**]$^{6-}$ was structurally characterized by SC-XRD as its $[NBu_4]_6$[**1**]·$4CH_3COCH_3$ salt (Figure 1 and Table 1). These crystals displayed ν_{CO} bands at 1985(vs), 1830(s), 1750(br) cm^{-1} as solid in nujol mull, and ν_{CO} at 1999(vs), 1873(s), 1856(s) cm^{-1} in CH_3CN solution. The differences in the ν_{CO} bands detected in the solid state and solution spectra were likely to be due to a slight rearrangement of the stereochemistry of the CO ligands after dissolution of the crystals in solution (see below).

Both compositional and substitutional disorders were observed in the structure of [**1**]$^{6-}$. The substitutional disorder was indicated by the fact that there were some positions within the metal cage of the cluster which may be occupied by either Ni or Pd (see below for details). Moreover, a free refinement of the occupancy factors of these sites indicated that [**1**]$^{6-}$ was actually a mixture of $[Ni_{21}Pd_{21}(CO)_{48}]^{6-}$ (62%) and $[Ni_{22}Pd_{20}(CO)_{48}]^{6-}$ (38%) (compositional disorder).

The 42-atom metal-core of [**1**]$^{6-}$ may be described as a five-layer close-packed stacking arrangement comprising 40 metal atoms capped by two additional metal atoms on two triangular faces related by an inversion centre (Figure 1). The close-packed layers adopted a *ccp* ABCAB configuration and contained 6, 9, 10, 9 and 6 metal atoms, respectively. Regarding the distribution of the Ni and Pd atoms on the metal core of the cluster, it was possible to distinguish four sets of positions. There were 16 positions (in green in Figure 1) which were fully occupied by Ni atoms; these positions displayed low M-M (3-7 bonds) and high M-CO (3-4, terminal and edge bridging) connectivities. There were, then, 18 positions (in purple in Figure 1) displaying high M-M (8-12) and low M-CO (0-2, edge or face bridging) connectivities which were fully occupied by Pd atoms. Among these, there were four fully interstitial positions. The third set comprised two Pd-rich positions at the centre of two (111) hexagonal faces (in yellow in Figure 1) with a refined Ni/Pd ratio of *ca.* 16:84 (M-M = 9; M-CO = 2, face bridging). Finally, there were six Ni-rich positions (in blue in Figure 1) with refined Ni/Pd ratios in the range Ni 82-87% and Pd 13-18% (M-M = 7; M-CO = 2-3, edge and face bridging). The structure contained 12 terminal, 18 edge bridging and 18 face bridging CO ligands. Ni-C and Pd-C contacts up to 2.31 and 2.50 Å, respectively, were considered as bonds on the basis of the reported covalent radii of C, Ni and Pd.[32] In the case of the 18 face bridging carbonyls, systematically one of the three M-C(O) contacts was rather longer than the other two contacts and, therefore, these were better described as intermediate between face and edge bridging. It was likely that in solution a slight rearrangement of the CO ligands occurred, since there was no evidence of face bridging carbonyls in the IR spectra recorded after dissolution of the crystals in organic solvents. Terminal carbonyls were bonded solely to Ni-atoms. Overall, there was a clear preference for Pd to occupy sites with high M-M and low M-CO connectivity, and Ni displayed the opposite trend.

[**1**]$^{6-}$ contained 522 cluster valence electrons (CVE), that corresponded to 261 (6n+9) filled molecular orbitals, in keeping with other high nuclearity Ni-Pt and Ni-Pd carbonyl clusters.[10,12,30,31]

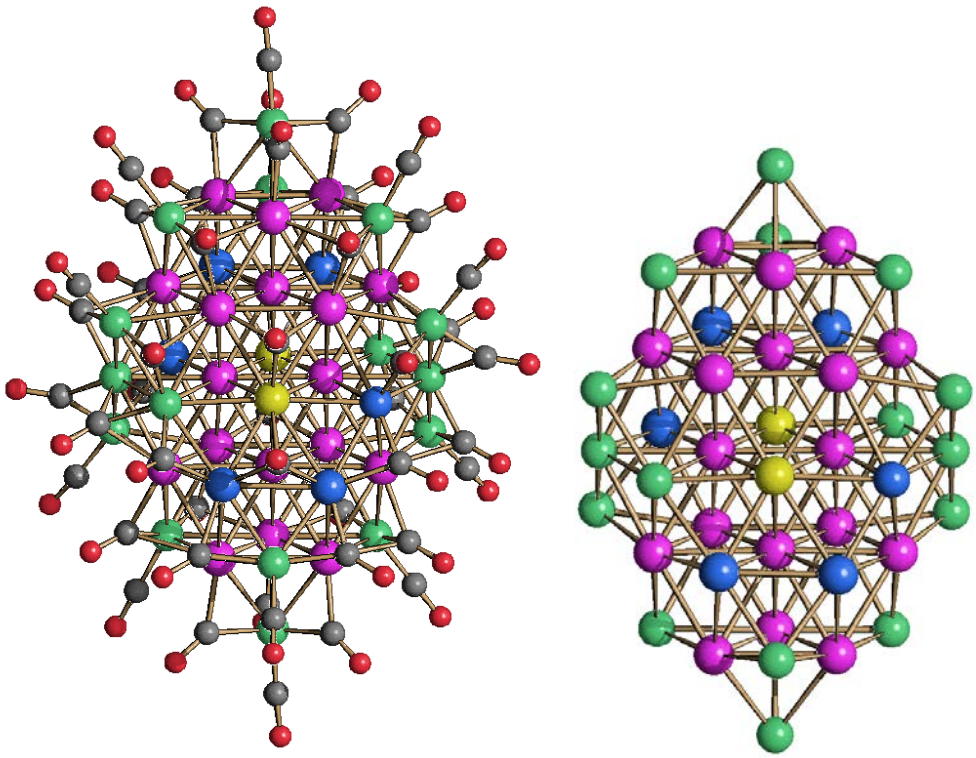

(a) (b)

Fig.1 (a) The molecular structure of $[\mathbf{1}]^{6-}$ and (b) its M_{42} metal core (green, Ni; purple, Pd; yellow, Ni/Pd≈ 16:84; blue, Ni/Pd≈ 82,85,87:18,15,13; grey, C; red, O).

Table 1 Main bond distances (Å) of $[Ni_{22-x}Pd_{20+x}(CO)_{48}]^{6-}$ (x = 0.62) ($[\mathbf{1}]^{6-}$), $[Ni_{29-x}Pd_{6+x}(CO)_{42}]^{6-}$ (x = 0.09) ($[\mathbf{2}]^{6-}$) and $[Ni_{29+x}Pd_{6-x}(CO)_{42}]^{6-}$ (x = 0.27) ($[\mathbf{3}]^{6-}$).

	Ni-Ni	**Ni-Pd**	**Pd-Pd**
$[\mathbf{1}]^{6-}$	2.4696(10)-2.95(2) Average 2.56(4)	2.40(4)-2.82(3) Average 2.67(5)	2.59(3)-2.9053(6) Average 2.773(19)
$[\mathbf{2}]^{6-}$	2.444(3)-2.725(3) Average 2.58(4)	2.35(7)-2.68(7) Average 2.61(9)	2.618(2)-2.7689(15) Average 2.68(3)
$[\mathbf{3}]^{6-}$	2.437(5)-2.732(3) Average 2.58(2)	2.324(17)-2.889(17) Average 2.65(5)	2.6256(19)-2.7585(13) Average 2.704(3)

Synthesis and structure of $[Ni_{29-x}Pd_{6+x}(CO)_{42}]^{6-}$ (x = 0.09) ($[\mathbf{2}]^{6-}$) and $[Ni_{29+x}Pd_{6-x}(CO)_{42}]^{6-}$ (x = 0.27) ($[\mathbf{3}]^{6-}$). $[\mathbf{2}]^{6-}$ and $[\mathbf{3}]^{6-}$ were obtained from the reaction of $[NEt_4]_2[Ni_6(CO)_{12}]$ with 0.6-0.7 equivalents of $Pd(Et_2S)_2Cl_2$ in CH_3CN and extracted in CH_3CN after work-up (see Experimental for details). It must be noticed that the synthesis of $[\mathbf{2}]^{6-}$ and $[\mathbf{3}]^{6-}$ differed from that of $[\mathbf{1}]^{6-}$ into three points: (1)

the stoichiometry of the reaction (0.6-0.7 *vs* 0.7-0.8 moles of $Pd(Et_2S)_2Cl_2$ per mole of $[Ni_6(CO)_{12}]^{2-}$ for $[\mathbf{2}]^{6-}$ and $[\mathbf{3}]^{6-}$ *vs* $[\mathbf{1}]^{6-}$); (2) the solvent employed, that is CH_3CN ($[\mathbf{2}]^{6-}$ and $[\mathbf{3}]^{6-}$) or CH_2Cl_2 ($[\mathbf{1}]^{6-}$); (3) the cation of $[Ni_6(CO)_{12}]^{2-}$, that is $[NEt_4]^+$ ($[\mathbf{2}]^{6-}$ and $[\mathbf{3}]^{6-}$) or $[NBu_4]^+$ ($[\mathbf{1}]^{6-}$). Point (3) was closely related to (2), since $[NEt_4]_2[Ni_6(CO)_{12}]$ was not soluble in CH_2Cl_2 whereas $[NBu_4]_2[Ni_6(CO)_{12}]$ was completely soluble in the same solvent, and both salts were soluble in CH_3CN. Conversely, $[\mathbf{2}]^{6-}$ and $[\mathbf{3}]^{6-}$ were obtained under very similar experimental conditions, that is, the same cation and solvent, and only slightly differed for the stoichiometric ratio of the reagents (see Experimental). These differences are so minimal that it was not very easy to control them, and the reactions for the synthesis of $[\mathbf{2}]^{6-}$ and $[\mathbf{3}]^{6-}$ must be carried out in a very controlled way. Indeed, $[\mathbf{2}]^{6-}$ and $[\mathbf{3}]^{6-}$ displayed the same structures (see below) and only showed minor differences in the composition, that is, $Ni_{28.91}Pd_{6.09}$ for $[\mathbf{2}]^{6-}$ and $Ni_{29.27}Pd_{5.73}$ for $[\mathbf{3}]^{6-}$.

$[\mathbf{2}]^{6-}$ and $[\mathbf{3}]^{6-}$ were structurally characterized by means of SC-XRD as their isomorphous $[NEt_4]_6[\mathbf{2}]\cdot 3CH_3CN\cdot$solv and $[NEt_4]_6[\mathbf{3}]\cdot 3CH_3CN\cdot$solv salts. The two anions were isostructural (Figure 2 and Table 1), and they only slightly differed for the Ni/Pd composition. Indeed, within the structures of $[\mathbf{2}]^{6-}$and $[\mathbf{3}]^{6-}$ there were six symmetry related positions (in yellow in Figure 2) which displayed substitutional Ni/Pd disorder. A free refinement of the unique independent position resulted in a Ni/Pd ratio of *ca.* 82:18 and 88:12 for $[\mathbf{2}]^{6-}$ and $[\mathbf{3}]^{6-}$, respectively. In the case of $[\mathbf{2}]^{6-}$, this corresponded to a mixture of $[Ni_{29}Pd_6(CO)_{42}]^{6-}$ (91%) and $[Ni_{28}Pd_7(CO)_{42}]^{6-}$ (9%). Considering the experimental errors in the refined occupancy factors, we can assume that this was an almost pure sample of $[Ni_{29}Pd_6(CO)_{42}]^{6-}$, displaying substitutional but not compositional disorder (or very limited).

Conversely, in the case of $[\mathbf{3}]^{6-}$, significant amounts of both $[Ni_{29}Pd_6(CO)_{42}]^{6-}$ (73%) and $[Ni_{30}Pd_5(CO)_{42}]^{6-}$ (27%) were present, indicative of both substitutional and compositional disorder. Overall, it may be assumed that the synthesis described resulted mainly in $[Ni_{29}Pd_6(CO)_{42}]^{6-}$, that can be accompanied by variable amounts of isostructural clusters differing for a few Ni/Pd atoms depending on the actual ratio of the reagents.

The molecular structures of $[\mathbf{2}]^{6-}$ and $[\mathbf{3}]^{6-}$ were based on a *hcp* M_{35} metal core composed of three compact ABA layers consisting of 10, 15 and 10 metal atoms respectively. This metal core closely resembled to that previously found in $[Cu_xNi_{35-x}(CO)_{40}]^{5-}$ (x = 3 or 5).[33] The nature of the latter Ni-Cu cluster was not completely known, since it was not possible to ascertain its precise composition. Based on the published data, the cluster could contain three or five Cu atoms.

The M_{35} metal core of pseudo-D_{3h} symmetry contained three interstitial metal atoms, nine metal atoms occupying the corner sites, 21 metal atoms in non-corner edge sites, and two metal atoms located at

the central 111 terrace site of the top and bottom 10-atom triangles. There were 12 octahedral and 26 tetrahedral holes within this *hcp* metal-core polyhedron.

A Pd_5 trigonal bipyramid (TBP), comprising the three interstitial and two terrace site metal atoms, was enclosed within this metal cage. These positions corresponded to metal sites with no CO coordination (three interstitial metal sites) or weakly bonded to μ_3-CO ligands (two sites at the central 111 terraces). The same positions were occupied by a Cu_5 TBP in $[Cu_xNi_{35-x}(CO)_{40}]^{5-}$ (x = 3 or 5), assuming x = 5.

Both structures contained 42 CO ligands, 9 in terminal positions, 18 edge bridging and 15 face bridging. Pd-atoms were no bonded to any CO or connected only to edge or face bridging CO ligands.

$[\mathbf{2}]^{6-}$ and $[\mathbf{3}]^{6-}$ contained 440 CVE. Thus, they were isoelectronic with $[Cu_xNi_{35-x}(CO)_{40}]^{5-}$ (x = 3 or 5), assuming x = 5. This corresponded to 220 (6n+10) filled molecular orbitals.

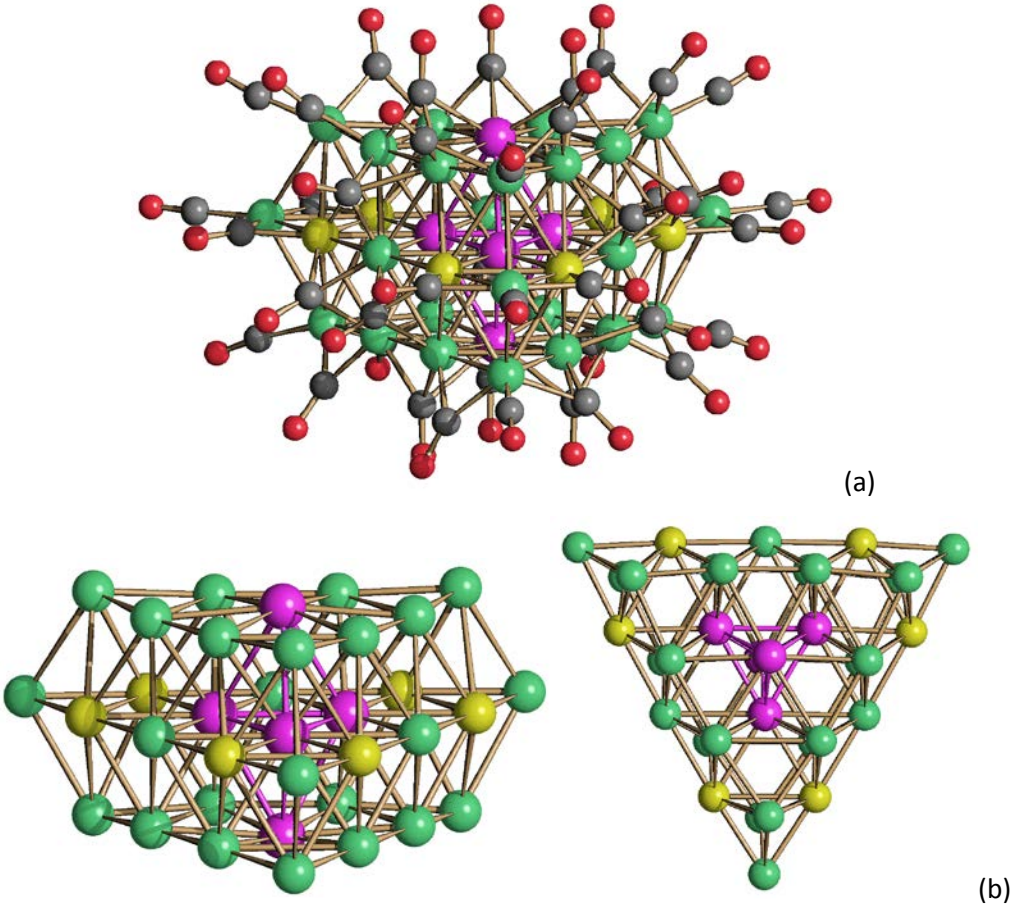

Fig.2 (a) The molecular structure of $[\mathbf{2}]^{6-}$ and $[\mathbf{3}]^{6-}$, and (b) two views of their M_{35} metal core (green, Ni; purple, Pd, yellow, Ni/Pd≈ 82:18 and 88:12 for $[\mathbf{2}]^{6-}$ and $[\mathbf{3}]^{6-}$, respectively; grey, C; red, O).

Electrochemistry and Infrared Spectro-electrochemistry

The redox properties of $[\mathbf{1}]^{6-}$ and $[\mathbf{2}]^{6-}$ were determined by means of electrochemical and spectroelectrochemical methods. This represented the first IR-SEC study of large Ni-Pd carbonyl clusters.

In many cases, we noted that the *in situ* IR spectroelectrochemical study of molecular metal carbonyl nanoclusters could provide interesting results in order to gain insight on the existence of different stable redox states, even when in the current/potential profile of the cyclic voltammetry experiments the current densities were very low leading to unresolved peaks.[34,35] So, the redox chemistry of $[\mathbf{1}]^{6-}$ was studied by *in situ* infrared spectroelectrochemistry (IR SEC) in CH_3CN solution containing $[N^nBu_4][PF_6]$ as supporting electrolyte. In particular, three chemically reversible redox couples were recognized from the analysis of the sequence of the vibrational spectra in the CO stretching region collected at constant time intervals during the potential cycling of the Pt working electrode between 0.0 and -1.5 V *vs*. Ag pseudo-reference electrode, at the scan rate of 1 mV s^{-1}. Two consecutive reductions were indicated by a progressive shift of both the terminal and bridging ν_{CO} bands of the cluster from 1999 and 1873 cm^{-1} to 1985 and 1857 cm^{-1} (lowering the potential from -0.8 to -1.2 V), and to 1971 and 1852 cm^{-1} (from -1.2 to -1.5 V) (Figure S1). Well-defined isosbestic points appeared in both cases, indicating the relative stability of the electrogenerated species. Moreover, the IR spectrum of the starting cluster was restored when the potential of the working electrode was returned to the initial value, pointing out that the reduced species were stable in the time scale of the SEC experiments.

A shift at higher wavenumbers (2014 and 1883 cm^{-1}) was observed on increasing the potential from -0.3 to 0.0 V (Figure S2), and also in this case the IR spectrum of $[\mathbf{1}]^{6-}$ was restored in the backward potential scan.

Overall, one oxidation and two reduction processes of the cluster were identified, and the IR spectra of four oxidation states of $[\mathbf{1}]^{6-}$ were selected (Figure 3). The stretching frequencies of the terminal (ν^t_{CO}) and bridging (ν^b_{CO}) carbonyl groups for each species were reported in Table 2.

By comparison of the stretching frequencies of terminal CO ligands belonging to the reversible redox states of the cluster, for all processes we observed a near-uniform shift of 14 cm^{-1}, suggesting a one-electron transfer for each redox exchange.[36]

Thus, the four long-lived species $[\mathbf{1}]^{5-/6-/7-/8-}$ were spectroscopically characterized, proving that the structure of $[\mathbf{1}]^{6-}$ was stable with a variable number of electrons. Both the terminal and bridging ν_{CO} bands kept their shape and relative intensity on changing the cluster charge, so we could presume that only minor structural changes regarding the stereochemistry of CO ligands, occurred in the time scale of SEC experiment.

Table 2 Infrared stretching frequencies (cm^{-1}) of the terminal (ν^t_{CO}) and bridging (ν^b_{CO}) carbonyl groups for $[\mathbf{1}]^n$ in CH_3CN as a function of the cluster charge *n*.

Cluster charge *n*	ν^t_{CO}	ν^b_{CO}
-5	2014	1883(sh), 1866
-6	1999	1873, 1856
-7	1985	1857
-8	1971	1852

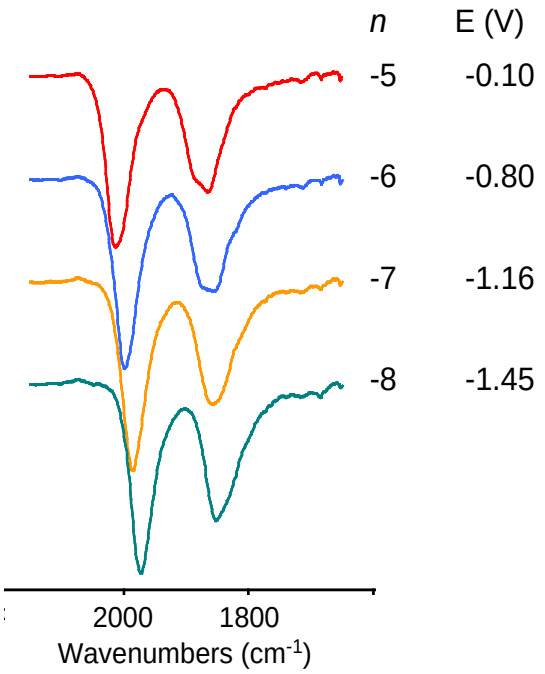

Fig.3 Selected infrared spectra of $[\mathbf{1}]^n$ as a function of the cluster charge *n* and of the potential E (*vs.* Ag pseudo-reference electrode), in CH_3CN containing 0.1 M $[N^nBu_4][PF_6]$. The absorptions of the solvent and the supporting electrolyte have been subtracted.

The electrochemical properties of $[\mathbf{2}]^{6-}$ were preliminarily investigated by cyclic voltammentry (CV) and differential pulse voltammetry (DPV) at a Pt electrode in $CH_3CN/[N^nBu_4][PF_6]$ solution at different scan rates, namely 5, 20, 50, 100 and 200 mV/s. Three subsequent cathodic steps could be detected between -0.9 and -1.8 V (*vs*. Ag/AgCl KCl sat), all having features of chemical reversibility on the cyclic voltammetric timescale (Figure S3). The peaks appeared broad and the electrochemical reversibility of the processes could not be assessed, while the current densities, although low, indicated for all the processes the same

number of exchanged electrons, presumably one. Concerning the anodic scan, increasing the potential between -0.9 and -0.4 V the current increased and one oxidation process was hardly identified.

The IR SEC in the same electrolyte showed that two chemically reversible reductions were followed by a further process which was complicated by a fast subsequent chemical reaction. In fact, from the IR spectra sequence recorded between -0.6 and -1.5 V (*vs* Ag pseudo-reference electrode) we were able to separate the spectra into two groups (Figure S4 (a) and (b)), each of them attributable to a reversible electron exchange, while, further decreasing the potential up to -1.8 V, a continuous shift at lower frequencies of both terminal and bridging CO ligands was accompanied by the appearance of the 2127 cm^{-1} band of dissolved CO (Figure S4 (c)), indicating the decomposition of the electrogenerated more reduced cluster, since in the reverse backscan at the initial potential new absorptions due to unknown products were observed in the IR spectrum. Thus, the third reduction, which appeared chemically reversible in the timescale of the CV, became irreversible in the timescale of the SEC experiment.

When the working electrode potential was increased from -0.6 to +0.2 V (*vs* Ag pseudo-reference electrode), a continuous shift of the two IR bands of $[\mathbf{2}]^{6-}$ at higher frequencies indicated an oxidation step. However, we failed to obtain the spectrum of only the oxidized $[\mathbf{2}]^{5-}$, since, before the complete disappearance of the starting cluster, a little shoulder at 2040 cm^{-1} attributable to $Ni(CO)_4$, pointed out the breaking of the cluster core (Figure S4 (d)). In this case the decomposition appeared relatively slow, and the starting spectrum of $[\mathbf{2}]^{6-}$ was almost completely restored in the reverse reduction backscan (Figure S5).

We attempted the spectral deconvolution of three spectra acquired during the oxidation of $[\mathbf{2}]^{6-}$, and before the appearance of the 2040 cm^{-1} shoulder, to assess the number of bands and the relative contribute of each to the overall spectra: by using peak fitting on Origin 2015 and multiple individual peaks, we obtained in all cases a good fitting by the combination of two bands at 1995 and 2010, in different ratios according to the direction of the potential scan (Figure S6) and the maximum area ratio was 58:42 in favour of the higher frequencies band. Therefore, we can confidently assign the 2010 cm^{-1} peak to terminal CO groups of a different and higher oxidation state.

Overall, one oxidation and two reduction processes of the cluster were identified by the SEC, and the IR spectra of four oxidation states of $[\mathbf{2}]^{n-}$ were selected (Figure 4). The stretching frequencies of the terminal (ν^{t}_{CO}) and bridging (ν^{b}_{CO}) carbonyl groups for each species were reported in Table 3. The charge of each species was assigned according to one-electron transfer for each redox exchange, as inferred by a near-uniform shift of 15 cm^{-1} of the stretching frequencies of terminal CO ligands for all the processes.

By the joint electrochemical/spectroelectrochemical study of $[\mathbf{2}]^{6-}$, four redox couples chemically reversible in the timescale of CV were identified; the three long-lived species $[\mathbf{2}]^{6-/7-/8-}$ and the relatively

unstable $[\mathbf{2}]^{5-}$ were spectroscopically characterized, proving that also the structure of $[\mathbf{2}]^{6-}$ was stable with a variable number of electrons.

Table 3 Infrared stretching frequencies (cm^{-1}) of the terminal (ν^{t}_{CO}) and bridging (ν^{b}_{CO}) carbonyl groups for $[\mathbf{2}]^{n}$ in CH_3CN as a function of the cluster charge *n*.

Cluster charge *n*	ν^{t}_{CO}	ν^{b}_{CO}
-5	2010	1882, 1866
-6	1995	1873, 1854sh
-7	1980	1860, 1840sh
-8	1963	1841

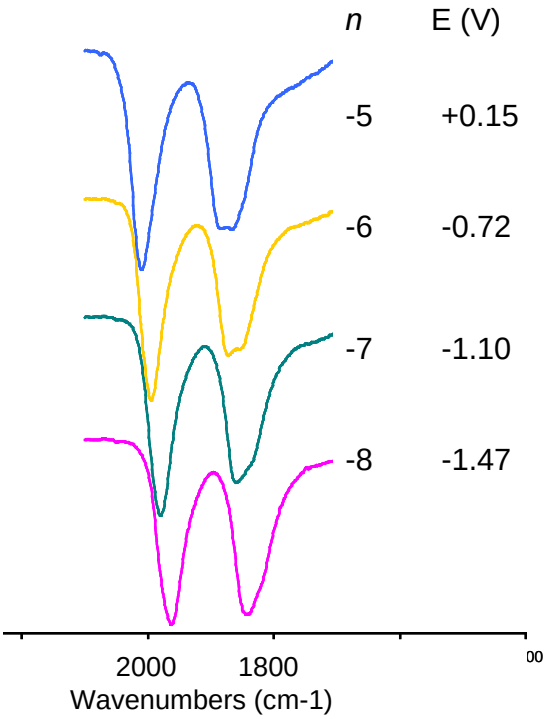

Fig.4 Selected infrared spectra of $[\mathbf{2}]^{n}$ as a function of the cluster charge *n* and of the potential E (*vs.* Ag pseudo-reference electrode), in CH_3CN containing 0.1 M $[N^{n}Bu_4][PF_6]$. The absorptions of the solvent and the supporting electrolyte have been subtracted.

Conclusions

The new redox active Ni-Pd carbonyl alloy nanoclusters $[\mathbf{1}]^{6-}$, $[\mathbf{2}]^{6-}$ and $[\mathbf{3}]^{6-}$ were obtained by redox condensation and their molecular structures determined by SC-XRD. Their compact metal cores were

essentially *ccp* for $[\mathbf{1}]^{6-}$ and *hcp* for $[\mathbf{2}]^{6-}$ and $[\mathbf{3}]^{6-}$, with maximum sizes 1.3 and 1.0 nm, respectively. By including also the CO ligands, their maximum dimensions increased up to 1.9 nm for $[\mathbf{1}]^{6-}$ and 1.5 nm for $[\mathbf{2}]^{6-}$ and $[\mathbf{3}]^{6-}$. Therefore, these high nuclearity metal carbonyl clusters might be described as molecular nanoclusters or ultra-small metal nanoparticles in accord to the present literature.[5,8,18-25,37-39]

The Ni-Pd distribution within the metal cores of these molecular alloy carbonyl nanoclusters was dictated by avoiding terminal Pd-CO bonding and minimizing Pd-CO coordination, as previously reported.[10-12] This led to site preference and partial metal segregation. Nonetheless, some substitutional and compositional disorder was detected, due to the presence of a few sites which could be occupied by either Ni or Pd atoms. As a consequence, mixtures of isostructural (and almost identical) clusters differing for the position and/or number of a few Ni/Pd atoms were obtained. Such disorder phenomena were common in larger alloy nanoparticles and bulk alloy phases. In view of the molecular nature of $[\mathbf{1}]^{6-}$, $[\mathbf{2}]^{6-}$ and $[\mathbf{3}]^{6-}$, it was possible to unravel the exact structure and composition of their metal cores. Thus, alloying metals at the molecular and sub-nanometric level might reveal such structural phenomena with atomic precision.[26,27]

From a synthetic point of view, all of these new clusters were obtained by redox condensation of the $[Ni_6(CO)_{12}]^{2-}$ carbonyl anion with Pd(II) complexes such as $Pd(Et_2S)_2Cl_2$.[8,18] Different products were obtained by systematically changing the stoichiometric ratio of the reagents, the solvent and the cation of $[Ni_6(CO)_{12}]^{2-}$. Redox condensation represents a general strategy largely employed for the synthesis of several metal carbonyl clusters, especially those displaying higher nuclearities.[8-13,17-21,30,31,34-36] The experimental conditions for the obtainment of $[\mathbf{1}]^{6-}$ compared to $[\mathbf{2}]^{6-}$ and $[\mathbf{3}]^{6-}$ were rather different and, therefore, it was quite straightforward to selectively obtain $[\mathbf{1}]^{6-}$ rather $[\mathbf{2}]^{6-}$ and $[\mathbf{3}]^{6-}$. Conversely, $[\mathbf{2}]^{6-}$ and $[\mathbf{3}]^{6-}$ were obtained under very similar experimental conditions, slightly differing only in the stoichiometric ratio of the reagents. Therefore, much care must be used for their synthesis and reproducibility.

Electrochemical and SEC experiments indicated that $[\mathbf{1}]^{6-}$ and $[\mathbf{2}]^{6-}$ were redox active, displaying, respectively, four and three stable oxidation states. Thus, they might be defined multivalent and behaved as electron sinks and molecular nanocapacitors.[8,30,35,36] This, in turn, indicated the incipient metallization of their metal cores that, in conjunction with the protecting effect of the CO layer, could reversibly accept and release electrons at well-defined potentials.

Multivalence in high nuclearity metal carbonyl clusters was not uncommon.[8,18] Nonetheless, the majority of the redox active clusters, so far reported, contained strong M-M, M-M' or M-X bonds (M, M' = transition metal, X = p-block element). This was usually achieved by using second and third row transition metals, such as Pt, Rh and Ir, in homometallic or bimetallic species, the latter also in the presence of first

row transition metals. Alternatively, p-block elements could be introduced resulting in multivalent carbonyl clusters, as well exemplified in the case of high nuclearity Ni-CO hetero-element clusters.[8,18,34-36,40]

In this respect, several redox active Ni-Pt carbonyl alloy nanoclusters were reported,[10,30,31] whereas it was somehow claimed that the strength of all bonds involving Pd was insufficient to stabilize different redox states in Ni-Pd carbonyl clusters.[8] Thus, the results herein described represented the first report on redox active Ni-Pd carbonyl alloy nanoclusters. Despite the fact that Pd-Pd, Pd-Ni and Pd-CO bonds were weaker than those involving Pt, the synergic effect of the two metals, as shown by the Ni-Pd distribution within their nanometric metal cores, was able to stabilize larger metal cages also with a variable number of electrons. In this sense, as shown by Dahl, high nuclearity Ni-Pd-CO and Pd-CO-PPh_3 clusters were somehow similar to thiol protected Au nanoclusters.[2,5,6,41]

Experimental

General procedures.

All reactions and sample manipulations were carried out using standard Schlenk techniques under nitrogen and in dried solvents. All the reagents were commercial products (Aldrich) of the highest purity available and used as received, except $[NR_4]_2[Ni_6(CO)_{12}]$ (R = Et, Bu) [42] and $Pd(Et_2S)_2Cl_2$ [43] which have been prepared according to the literature. Analyses of C, H and N were obtained with a Thermo Quest Flash EA 1112NC instrument. Analysis of Ni and Pd were performed by microwave plasma-atomic emission spectrometry on a Agilent 4210 MP-AES instrument. IR spectra were recorded on a Perkin Elmer Spectrum One interferometer in CaF_2 cells. Structure drawings have been performed with SCHAKAL99.[44]

WARNING: CO and $Ni(CO)_4$ may be generated during manipulation of these compounds. All the operations must be carried out under a well-ventilated fume hood.

Synthesis of $[NBu_4]_6$[1]·$4CH_3COCH_3$ (x = 0.62)

A solution of $Pd(Et_2S)_2Cl_2$ (0.293 g, 0.821 mmol) in CH_2Cl_2 (12 mL) was added in small portions to a solution of $[NBu_4]_2[Ni_6(CO)_{12}]$ (1.257 g, 1.072 mmol) in CH_2Cl_2 (30 mL) over a period of 6 h. The resulting mixture was stirred at room temperature for 24 h and, then, the solvent removed *in vacuo*. The residue was washed with H_2O (3×20 mL), toluene (3×20 mL), CH_2Cl_2 (20 mL), thf (20 mL), and extracted with acetone (20 mL). Crystals of $[NBu_4]_6$[**1**]·$4CH_3COCH_3$ (x = 0.62) suitable for X-ray analyses were obtained bylayering n-hexane (40 mL) on the acetone solution (yield 0.136 g, 53 % based on Pd, 7 % based on Ni).

$C_{156}H_{240}N_6Ni_{21.38}O_{52}Pd_{20.62}$(6481.20): calcd. C 28.91, H 3.73, N 1.30, Ni 19.35, Pd 33.87; found: C 29.10, H 3.92, N 1.04, Ni 19.54, Pd 33.68. IR (nujol, 293 K) ν_{CO}: 1985(vs), 1830(s), 1750(br) cm^{-1}. IR (CH_2Cl_2, 293 K)

ν_{CO}: 2004(vs), 1877(s) cm^{-1}. IR (acetone, 293 K) ν_{CO}: 1999(vs), 1882(s), 1863(sh) cm^{-1}. IR (CH_3CN, 293 K) ν_{CO}: 1999(vs), 1873(s), 1856(s) cm^{-1}. IR (dmso, 293 K) ν_{CO}: 1995(vs), 1867(s) cm^{-1}.

Synthesis of $[NEt_4]_6$[2]·3CH_3CN·solv

A solution of $Pd(Et_2S)_2Cl_2$ (0.330 g, 0.927 mmol) in CH_3CN (20 mL) was added in small portions to a solution of $[NEt_4]_2[Ni_6(CO)_{12}]$ (1.320 g, 1.390 mmol) in CH_3CN (30 mL) over a period of 6 h. The resulting mixture was stirred at room temperature for 24 h and, then, the solvent removed *in vacuo*. The residue was washed with H_2O (3×20 mL), toluene (3×20 mL), thf (20 mL), acetone (20 mL), and extracted with CH_3CN (20 mL). Crystals of $[NEt_4]_6$[**2**]·CH_3CN·solv suitable for X-ray analyses were obtained by layering n-hexane (3 mL) and di-iso-propyl-ether (40 mL) on the CH_3CN solution (yield 0.412 g, 61 % based on Pd, 32% based on Ni).

$C_{95}H_{129}N_9Ni_{28.91}O_{42}Pd_{6.09}$ (4414.11): calcd. C 25.85, H 2.95, N 2.86, Ni 38.44, Pd 14.68; found: C 26.03, H 3.12, N 3.04, Ni 38.75, Pd 14.39. IR (nujol, 293 K) ν_{CO}: 2000(vs), 1854(s), 1744(br) cm^{-1}. IR (CH_3CN, 293 K) ν_{CO}: 1995(vs), 1873(s), 1854(sh) cm^{-1}. IR (dmf, 293 K) ν_{CO}: 1988(vs), 1873(s), 1851(sh) cm^{-1}.

Synthesis of $[NEt_4]_6$[3]·3CH_3CN·solv

A solution of $Pd(Et_2S)_2Cl_2$ (0.330 g, 0.927 mmol) in CH_3CN (20 mL) was added in small portions to a solution of $[NEt_4]_2[Ni_6(CO)_{12}]$ (1.380 g, 1.453 mmol) in CH_3CN (30 mL) over a period of 6 h. The resulting mixture was stirred at room temperature for 24 h and, then, the solvent removed *in vacuo*. The residue was washed with H_2O (3×20 mL), toluene (3×20 mL), thf (20 mL), acetone (20 mL), and extracted with CH_3CN (20 mL). Crystals of $[NEt_4]_6$[**3**]·CH_3CN·solv suitable for X-ray analyses were obtained by layering n-hexane (3 mL) and di-iso-propyl-ether (40 mL) on the CH_3CN solution (yield 0.385 g, 54 % based on Pd, 29% based on Ni).

$C_{95}H_{129}N_9Ni_{29.27}O_{42}Pd_{5.73}$ (4409.19): calcd. C 25.88, H 2.95, N 2.86, Ni 38.96, Pd 13.83; found: C 25.99, H 2.78, N 3.01, Ni 38.81, Pd 14.21. IR (nujol, 293 K) ν_{CO}: 2005(vs), 1835(s), 1744(br) cm^{-1}. IR (CH_3CN, 293 K) ν_{CO}: 1999(vs), 1873(s), 1849(sh) cm^{-1}.

X-ray Crystallographic Study.

Crystal data and collection details for $[NBu_4]_6$[**1**]·4CH_3COCH_3, $[NEt_4]_6$[**2**]·3CH_3CN·solv and $[NEt_4]_6$[**3**]·3CH_3CN·solv are reported in Table S1. The diffraction experiments were carried out on a Bruker APEX II diffractometer equipped with a PHOTON100 detector using Mo–Kα radiation. Data were corrected for Lorentz polarization and absorption effects (empirical absorption correction SADABS).[45] Structures were solved by direct methods and refined by full-matrix least-squares based on all data using F^2.[46] Hydrogen

atoms were fixed at calculated positions and refined by a riding model. All non-hydrogen atoms were refined with anisotropic displacement parameters, unless otherwise stated.

$[NBu_4]_6[1]\cdot 4CH_3COCH_3$: The asymmetric unit of the unit cell contains half of a cluster anion (located on an inversion centre), three $[NBu_4]^+$ cations and two CH_3COCH_3 molecules located on general positions. The positions occupied by M(3), M(8), M(17) and M(21) are disordered Ni/Pd. These have been refined applying dummy atoms constraints (EADP and EXYZ lines in SHLEXL) resulting in the following refined occupancy factors: M(3) = 0.816(6) Ni and 0.184(6) Pd; M(8) = 0.867(6) Ni and 0.133(6) Pd; M(17) = 0.850(6) Ni and 0.150(6) Pd; M(21) = 0.158(6) Ni and 0.842(6) Pd. Similar *U* parameter restraints have been applied to the $[NBu_4]^+$ cations and CH_3COCH_3 molecules (SIMU command in SHELXL, s.u. 0.01). Restraints to bond distances were applied as follow (s.u. 0.01): 1.47 Å for C–N and 1.53 Å for C–C in $[NBu_4]^+$; 1.21 Å for C–O and 1.51 Å for C–C in CH_3COCH_3.

$[NEt_4]_6[2]\cdot 3CH_3CN\cdot$solv and $[NEt_4]_6[3]\cdot 3CH_3CN\cdot$solv: The asymmetric unit of the unit cell contains one sixth of a cluster anion (located on Wickoff position *d*, site symmetry 3.2), one $[NEt_4]^+$ cation (located on a general position) and half of a CH_3CN molecule disordered over two equally populated symmetry related (by an inversion centre) positions. The unit cell contains an additional total potential solvent accessible void of 515 and 495 $Å^3$ (*ca*. 8% of the Cell Volume), which is likely to be occupied by further highly disordered CH_3CN molecules. These voids have been treated using the SQUEEZE routine of PLATON.[47] The $[NEt_4]^+$ cation is disordered and, thus, it has been split into two positions and refined with one occupancy parameter per disordered group. Some CO ligands in the cluster anion are disordered; the disorder model adopted includes four CO ligands in PART 1 and three CO ligands in PART 2, all with occupancy factor 0.5. The position occupied by M(3) is disordered Ni/Pd. This has been refined applying dummy atoms constraints (EADP and EXYZ lines in SHLEXL) resulting in the following refined occupancy factor: M(3) = 0.819(14) Ni and 0.181(18) Pd; M(3) = 0.878(11) Ni and 0.122(11) Pd, for the two structures, respectively. The C and N atoms of the $[NEt_4]^+$ cation and CH_3CN molecule have been restrained to have similar *U* parameters (SIMU command in SHELXL, s.u. 0.01). Restraints to bond distances were applied as follow (s.u. 0.02): 1.14 Å for C–N and 1.47 Å for C–C in CH_3CN.

CCDC 1980407-1980409 contain the supplementary crystallographic data for this paper.

Electrochemical and spectroelectrochemical measurements.

Electrochemical measurements were performed with a PalmSens4 instrument interfaced to a computer employing PSTrace5 electrochemical software. CV measurements were carried out at room temperature under Ar in CH_3CN solutions containing $[N^nBu_4][PF_6]$ (0.1 mol dm^{-3}) as the supporting electrolyte. HPLC

grade CH_3CN (Sigma-Aldrich) was stored under argon over 3-Å molecular sieves. Electrochemical grade $[N^nBu_4][PF_6]$ was purchased from Fluka and used without further purification. Cyclic voltammetry was performed in a three-electrode cell, the working and the counter electrodes consisted of a Pt disk and a Pt gauze, respectively, both sealed in a glass tube. An Ag/AgCl, KCl sat electrode mounted with a salt bridge containing the $CH_3CN/[N^nBu_4][PF_6]$ electrolyte and separated by a Vycor frit was employed as a reference. The three-electrode home-built cell was pre-dried by heating under vacuum and filled with argon. The Schlenk-type construction of the cell maintained anhydrous and anaerobic conditions. The solution of supporting electrolyte, prepared under argon, was introduced into the cell and the CV of the solvent was recorded. The analyte was then introduced and voltammograms were recorded. Under the present experimental conditions, the one-electron oxidation of ferrocene occurs at E° = +0.42 V *vs* Ag/AgCl. Infrared (IR) spectroelectrochemical measurements were carried out using an optically transparent thin-layer electrochemical (OTTLE) cell [48] equipped with CaF_2 windows, platinum mini-grid working and auxiliary electrodes and silver wire pseudo-reference electrode. During the microelectrolysis procedures, the electrode potential was controlled by a PalmSens4 instrument interfaced to a computer employing PSTrace5 electrochemical software. Argon-saturated CH_3CN solutions of the compound under study, containing $[N^nBu_4][PF_6]$ 0.1 M as the supporting electrolyte, were used. The *in situ* spectroelectrochemical experiments have been performed by collecting spectra of the solution at constant time intervals during the oxidation or reduction obtained by continuously increasing or lowering the initial working potential at a scan rate of 1.0 or 0.5 mV/sec. IR spectra were recorded on a Perkin-Elmer Spectrum 100 FT-IR spectrophotometer.

ACKNOWLEDGMENTS

We thank the University of Bologna for financial support. T.F. acknowledges the financial support of the University of Pisa. We thank the referees for useful suggestions in revising the manuscript.

References

(1) K. C. C. Kharas and L. F. Dahl, *Adv. Chem. Phys.*, 1988, **70**, 1-43.

(2) E. G. Mednikov and L. F. Dahl, *J. Chem. Educ.*, 2009, **86**, 1135.

(3) C. E. Housecroft, M. E. O'Neil, K. Wade and B. C. Smith, *J. Organomet. Chem.*, 1981, **213**, 35-43.

(4) (a) C. Wang, S. C. Siu, G. Hwang, F. Aubke, C. Bach, B. Bley, M. Bodenbinder and H. Wilner, *Can. J. Chem.*, 1996, **74**, 1952-1958; (b) H. Wilner, M. Bodenbinder, R. Bröchler, G.

Hwang, S. J. Retting, J. Trotter, B. von Ahsen, U. Westphal, V. Jonas, W. Thiel and F. Aubke, *J. Am. Chem. Soc.*, 2001, **123**, 588-602.

(5) E. G. Mednikov and L. F. Dahl, *Phil. Trans. R. Soc. A*, 2010, **368**, 1301-1322.

(6) J. D. Erickson, E. G. Mednikov, S. A. Ivanov and L. F. Dahl, *J. Am. Chem. Soc.*, 2016, **138**, 1502-1505.

(7) A. B. Anderson and M. K. Awad, *J. Am. Chem. Soc.*, 1985, **107**, 7854-7857.

(8) C. Femoni, M. C. Iapalucci, F. Kaswalder, G. Longoni and S. Zacchini, *Coord. Chem. Rev.*, 2006, **250**, 1580-1604.

(9) (a) I. Ciabatti, C. Femoni, M. Gaboardi, M. C. Iapalucci, G. Longoni, D. Pontiroli, M. Riccò and S. Zacchini, *Dalton Trans.*, 2014, **43**, 4388-4399; (b) B. Berti, I. Ciabatti, C. Femoni, M. C. Iapalucci and S. Zacchini, *ACS Omega*, 2018, **3**, 13239-13250.

(10) C. Femoni, M. C. Iapalucci, G. Longoni, P. H. Svensson, P. Zanello and F. Fabrizi de Biani, *Chem. Eur. J.*, 2004, **10**, 2318-2326.

(11) N. T. Tran, M. Kawano, D. R. Powell and L. F. Dahl, *J. Chem. Soc., Dalton Trans.*, 2000, 4138-4144.

(12) C. Femoni, M. C. Iapalucci, G. Longoni, P. H. Svensson and J. Wolowska, *Angew. Chem. Int. Ed.*, 2000, **39**, 1635-1637.

(13) A. F. Masters and J. T. Meyer, *Polyhedron*, 1995, **14**, 339-365.

(14) (a) A. L. Luna, D. Dragoe, K. Wang, P. Beaunier, E. Kowalska, B. Ohtani, D. Bahena Uribe, M. A. Valenzuela, H. Remita and C. Colbeau-Justin, *J. Phys. Chem. C*, 2017, **121**, 14302-14311; (b) J. Zhang and C. Zhao, *ACS Catal.*, 2016, **6**, 4512-4525.

(15) (a) L. Feng, H. Chong, P. Li, J. Xiang, F. Fu, S. Yang and H. Sheng, *J. Phys. Chem. C*, 2015, **119**, 11511-11515; (b) B. Sen, S. Kuzu, E. Demir, S. Akocak and F. Sen, *Int. J. Hydrogen Energy*, 2017, **42**, 23276-23283.

(16) (a) J. S. Feeley, A. Yu Stakheev, F. A. P. Cavalcanti and W. M. H. Sachtler, *J. Catal.*, 1992, **136**, 182-196; (b) P. Lu, T. Teranishi, K. Asakura, M. Miyake and N. Toshima, *J. Phys. Chem. B*, 1999, **103**, 9673-9682; (c) P. Hermann, D. Simon and B. Bigot, *Surf. Sci.*, 1996, **350**, 301-314.

(17) N. T. Tran, M. Kawano, D. R. Powell, R. K. Hayashi, C. F. Campana and L. F. Dahl, *J. Am. Chem. Soc.*, 1999, **121**, 5945-5952.

(18) S. Zacchini, *Eur. J. Inorg. Chem.*, 2011, 4125-4145.

(19) I. Ciabatti, C. Femoni, M. C. Iapalucci, G. Longoni and S. Zacchini, *J. Clust. Sci.*, 2014, **25**, 115-146.

(20) C. Femoni, M. C. Iapalucci, S. Ruggieri and S. Zacchini, *Acc. Chem. Res.*, 2018, **51**, 2748-2755.

(21) I. Ciabatti, C. Femoni, M. C. Iapalucci, S. Ruggieri and S. Zacchini, *Coord. Chem. Rev.*, 2018, **355**, 27-38.

(22) R. Jin, C. Zeng, M. Zhou and Y. Chen, *Chem. Rev.*, 2016, **116**, 10346-10413.

(23) I. Chakraborty and T. Pradeep, *Chem. Rev.*, 2017, **117**, 8208-8271.

(24) (a) Q. Yao, T. Chen, X. Yuan and J. Xie, *Acc. Chem. Res.*, 2018, **51**, 1338-1348; (b) S. Takano, S. Hasegawa, M. Suyama and T. Tsukuda, *Acc. Chem. Res.*, 2018, **51**, 3074-3083.

(25) (a) Z. Lei, X. -K. Wan, S. -F. Yuan, Z. -J. Guan and Q.- M. Wang, *Acc. Chem. Res.*, 2018, **51**, 2465-2474; (b) K. Konishi, M. Iwasaki and Y. Shichibu, *Acc. Chem. Res.*, 2018, **51**, 3125-3133.

(26) S. Hossain, Y. Niihori, L. V. Nair, B. Kumar and W. Kurashige, *Acc. Chem. Res.*, 2018, **51**, 3114-3124.

(27) S. Wang, Q. Li, X. Kang and M. Zhu, *Acc. Chem. Res.*, 2018, **51**, 2784-2792.

(28) J. A. Rodriguez, *Surf. Sci. Rep.*, 1996, **24**, 223-287.

(29) P. H. T. Philipsen, E. van Lenthe, J. G. Snijders and E. J. Baerends, *Phys. Rev. B*, 1997, **56**, 13556-13562.

(30) F. Fabrizi De Biani, C. Femoni, M. C. Iapalucci, G. Longoni, P. Zanello and A. Ceriotti, *Inorg. Chem.*, 1999, **38**, 3721-3724.

(31) F. Demartin, F. Fabrizi de Biani, C. Femoni, M. C. Iapalucci, G. Longoni, P. Macchi and P. Zanello, *J. Cluster Sci*., 2001, **12**, 61-74.

(32) B. Cordero, V. Gómez, A. E. Platero-Prats, M. Revés, J. Echeverría, E. Cremades, F. Barrágan and S. Alvarez, *Dalton Trans.*, 2008, 2832-2838.

(33) P. D. Mlynek, M. Kawano, M. A. Kozee and L. F. Dahl, *J. Clust. Sci.*, 2001, **12**, 313-338.

(34) C. Capacci, I. Ciabatti, C. Femoni, M. C. Iapalucci, T. Funaioli, S. Zacchini andV. Zanotti, *Inorg. Chem.*, 2018, **57**, 1136-1147.

(35) E. Cattabriga, I. Ciabatti, C. Femoni, T. Funaioli, M. C. Iapalucci and S. Zacchini, *Inorg. Chem.*, 2016, **55**, 6068-6079.

(36) D. Collini, F. Fabrizi de Biani, D. S. Dolzhnikov, C. Femoni, M. C. Iapalucci, G. Longoni, C. Tiozzo, S. Zacchini and P. Zanello, *Inorg. Chem.,* 2011, **50**, 2790-2798.

(37) M. R. Narouz, K. M. Osten, P. J. Unsworth, R. W. Y. Man, K. Salorinne, S. Takano, R. Tomihara, S. Kaappa, S. Malola, C. -T. Dinh, J. D. Padmos, K. Ayoo, P. J. Garrett, M. Nambo, J. H. Horton, E. H. Sargent, H. Häkkinen, T. Tsukuda and C. M. Crudden, *Nature Chem.,* 2019, **11**, 419-425.

(38) M. Zhou, T. Higaki, Y. Li, C. Zeng, Q. Li, M. Y. Sfeir and R. Jin, *J. Am. Chem. Soc.,* 2019, **141**, 19754-19764.

(39) X. Du and R. Jin, *ACS Nano,* 2019, **13**, 7383-7387.

(40) I. Ciabatti, C. Femoni, T. Funaioli, M. C. Iapalucci, S. Merighi and S. Zacchini, *J. Organomet. Chem.,* 2017, **849-850**, 299-305.

(41) E. G. Mednikov and L. F. Dahl *Small*,2008, **4**, 534-537.

(42) (a) J. C. Calabrese, L. F. Dahl, A. Cavalieri, P. Chini, G. Longoni and S. Martinengo, *J. Am. Chem. Soc.*,1974, **96**, 2616-2618; (b) G. Longoni, P. Chini and A. Cavalieri, *Inorg. Chem.,* 1976, **15**, 3025-3029.

(43) D. R. Fahey, *J. Chem. Soc., Chem. Commun.,* 1970, 417a-417a.

(44) E. Keller, SCHAKAL99, University of Freiburg, Germany, **1999**.

(45) G. M. Sheldrick, SADABS, Program for empirical absorption correction; University of Göttingen: Germany, **1996**.

(46) G. M. Sheldrick, *Acta Cryst.,* 2015, **C71**, 3-8.

(47) (a) A. L. Spek, *J. Appl. Cryst.,* 2003, **36**, 7-13; (b) A. L. Spek, *Acta Cryst.*, 2009, **D65**, 148-155.

(48) M. Krejčik, M. Daněk, F. Hartl, *J. Electroanal. Chem.,* 1991, **317**, 179-187.

Table of contents

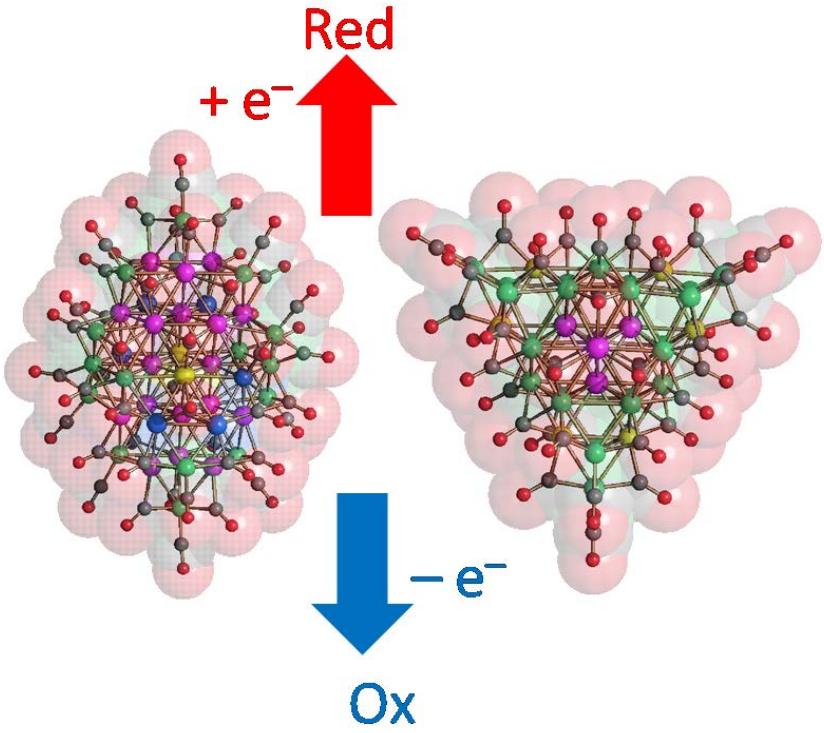

Redox active molecular Ni-Pd alloy nanoclusters were obtained by redox condensation, their total structures and metal distribution determined by X-ray crystallography, and their electron-sink behavior ascertained by electrochemical studies.